The Dependence of Atomic Oxygen Undercutting of Protected Polyimide Kapton® H Upon Defect Size

Aaron Snyder and Kim K. de Groh
Glenn Research Center, Cleveland, Ohio

Since its founding, NASA has been dedicated to the advancement of aeronautics and space science. The NASA Scientific and Technical Information (STI) Program Office plays a key part in helping NASA maintain this important role.

The NASA STI Program Office is operated by Langley Research Center, the Lead Center for NASA's scientific and technical information. The NASA STI Program Office provides access to the NASA STI Database, the largest collection of aeronautical and space science STI in the world. The Program Office is also NASA's institutional mechanism for disseminating the results of its research and development activities. These results are published by NASA in the NASA STI Report Series, which includes the following report types:

- TECHNICAL PUBLICATION. Reports of completed research or a major significant phase of research that present the results of NASA programs and include extensive data or theoretical analysis. Includes compilations of significant scientific and technical data and information deemed to be of continuing reference value. NASA's counterpart of peer-reviewed formal professional papers but has less stringent limitations on manuscript length and extent of graphic presentations.

- TECHNICAL MEMORANDUM. Scientific and technical findings that are preliminary or of specialized interest, e.g., quick release reports, working papers, and bibliographies that contain minimal annotation. Does not contain extensive analysis.

- CONTRACTOR REPORT. Scientific and technical findings by NASA-sponsored contractors and grantees.

- CONFERENCE PUBLICATION. Collected papers from scientific and technical conferences, symposia, seminars, or other meetings sponsored or cosponsored by NASA.

- SPECIAL PUBLICATION. Scientific, technical, or historical information from NASA programs, projects, and missions, often concerned with subjects having substantial public interest.

- TECHNICAL TRANSLATION. English-language translations of foreign scientific and technical material pertinent to NASA's mission.

Specialized services that complement the STI Program Office's diverse offerings include creating custom thesauri, building customized data bases, organizing and publishing research results . . . even providing videos.

For more information about the NASA STI Program Office, see the following:

- Access the NASA STI Program Home Page at *http://www.sti.nasa.gov*

- E-mail your question via the Internet to help@sti.nasa.gov

- Fax your question to the NASA Access Help Desk at 301–621–0134

- Telephone the NASA Access Help Desk at 301–621–0390

- Write to:
  NASA Access Help Desk
  NASA Center for AeroSpace Information
  7121 Standard Drive
  Hanover, MD 21076

The Dependence of Atomic Oxygen Undercutting of Protected Polyimide Kapton® H Upon Defect Size

Aaron Snyder and Kim K. de Groh
Glenn Research Center, Cleveland, Ohio

National Aeronautics and
Space Administration

Glenn Research Center

Available from

NASA Center for Aerospace Information
7121 Standard Drive
Hanover, MD 21076

National Technical Information Service
5285 Port Royal Road
Springfield, VA 22100

Available electronically at http://gltrs.grc.nasa.gov/GLTRS

THE DEPENDENCE OF ATOMIC OXYGEN UNDERCUTTING OF PROTECTED POLYIMIDE KAPTON® H UPON DEFECT SIZE

Aaron Snyder and Kim K. de Groh
National Aeronautics and Space Administration
Glenn Research Center
Cleveland, Ohio 44135

ABSTRACT—Understanding the behavior of polymeric materials when exposed to the low-Earth-orbit (LEO) environment is important in predicting performance characteristics such as in-space durability. Atomic oxygen (AO) present in LEO is known to be the principal agent in causing undercutting erosion of SiO_x protected polyimide Kapton® H film, which serves as a mechanically stable blanket material in solar arrays. The rate of undercutting is dependent on the rate of arrival, directionality and energy of the AO with respect to the film surface. The erosion rate also depends on the distribution of the size of defects existing in the protective coating. This paper presents results of experimental ground testing using low energy, isotropic AO flux together with numerical modeling to determine the dependence of undercutting erosion upon defect size.

1. INTRODUCTION

Thin protective films, such as SiO_x where $1.9 < x < 2.0$, are commonly used to protect polymers from erosion by energetic (4.5 eV) AO in LEO. However, defects in the coatings exist which allow the base polymer to be attacked causing erosion of the polymer substrate with subsequent gradual loss in its mechanical integrity. The durability of protected polymeric materials is predominantly dependent on the extent of AO undercutting at defect sites in the coating. Defect sites are typically manifested as pin windows, scratches, or cracks in the coating. In this paper the AO durability of the polyimide Kapton® H, which serves as a mechanically stable blanket material in solar arrays, is examined by investigating undercutting erosion below pin-window defects. Evaluating the in-space protective quality of coatings based on ground-test results using an AO plasma (~0.04 eV) is not simple due to differences between the two environments in AO energy, flux directionality and energy distribution. To provide better evaluation, more faithful characterizations of AO reactions with polymers are needed. Advanced modeling requires additional understanding of the mechanisms controlling undercutting at defect sites. Important aspects of cavity evolution can be studied without knowing the detailed nature of the erosion process. Prior investigations [1-4] have yielded valuable information on cavity shape, size, and distribution. This information has guided revision of the computational models used to predict undercutting.

Recently, cavity evolution occurring in protected Kapton®, exposed to an effective fluence of about 2×10^{22} atoms/cm² in a plasma asher, was investigated and results reported [5]. This fluence level produced numerous cavities several times wider than the film thickness, providing a broad range of cavities to be studied. For recent information focusing on smaller cavities, including novel rendering techniques, see [6].

Because much of the present work is an extension of [5], its primary findings are briefly reviewed here. Numerous cavities occurring beneath pin-window defects in the exposed upper protective coating were monitored using optical microscopy. Growth was documented by recording variation of cavity diameter with AO fluence. Three basic geometric models were used to estimate cavity volume. The models estimate volumes based on cavity diameters measured adjacent to the upper protective coating and the lower coating. It was found that the volumes of the smaller cavities increased less than linearly, whereas the volumes of larger-volume sites increased greater than linearly with AO fluence. It was determined for a particular cavity that its growth is adequately modeled as a simple power function of fluence; better modeling is achieved by taking into account the variation occurring in key geometrical ratios once the lower protective coating is reached. In addition, it was observed by scanning electron microscope (SEM) examination of some of the above defect sites that defect size is a factor in determining cavity shape. In general, and as expected, preliminary results indicated that larger defects produce larger cavities.

Although other factors influence cavity evolution, the parameter perceived to play the greatest role in site-to-site variation in cavity evolution is the defect size; it is important to have a clear understanding of how cavity evolution is influenced by defect size. The goal of this study is to correlate the variation in cavity growth with defect size. To supplement the information obtained from sites studied at successive fluence intervals, additional undercutting sites were identified and optically measured to determine cavity volume at final fluence. SEM measurements were made of the defects at many of these sites. Volume was calculated assuming a linear-arc cavity wall profile. The ratio of the volume erosion at each defect to the volume erosion due to an equivalent fluence of AO at an identical area of unprotected Kapton® is assessed in terms of the cavity defect size. This normalized erosion is denoted the **gain,** and it establishes a convenient metric for undercutting erosion. Numerical calculations of cavity growth were also made using an axisymmetric computational model to simulate undercutting erosion. In the results and discussion section, experimental and numerically calculated erosion gains are compared. Given knowledge of the gain for different defects sizes, and provided the approximate distribution of defects by size over a typical area of film is known [7], overall erosion rates of protected material can be estimated. It is hoped this information can be used in the future to predict in-space AO durability as based on ground-laboratory data.

2. EXPERIMENTAL

The study used a 13.56-MHz SPI Plasma Prep-II operated with air. This type of asher produces plasma by the use of a low pressure, radio-frequency induced, gaseous discharge. The optical measurements were made using an Olympus SZH microscope. Coordinates of specific cavity sites after each fluence increment were obtained using a xy-positioner. High magnification (up to 20K x) micrographs of defect sites in the glass protective coating were made using a JEOL JMS-6100 scanning electron microscope, after sputter coating the sample with a thin (~7.5 nm) layer of Pd to prevent excessive accumulation of electrostatic charge. The areas of site defects recorded on the SEM micrographs were measured using a mechanical planimeter.

The Kapton® sample was cut from a sheet of 0.0254-mm thickness Sheldahl-701664, covered on both faces with 0.13 microns (1300 Å) of SiO_x where $1.9 < x < 2.0$. Prior to ashing, the sample was

mounted on a 2.5 by 7.5-cm slide and trimmed to this size. It was fastened by double adhesive tape along its periphery, designed to permit exposure to only the upper surface. During each ashing session, the sample was accompanied by a fresh 0.125-mm thick by 25-mm diameter Kapton® witness coupon to monitor mass loss and provide fluence history.

Undercutting sites were selected with emphasis on shape circularity. Cavity diameters were determined by measuring the silhouette produced by transmitted light from below. Figure 1 shows a image produced from an optical microscope photograph that reveals the cavity of site 9. The black annular area, concentric with the site's center, corresponds to the sloped wall of the undercut cavity. Thus, the white inner portion represents the exposed silhouette of the lower protective coating. Similarly, the outer boundary of the black annular ring corresponds to the silhouette of the exposed upper coating containing the defect. This defect is shown in figure 2. Although it is composed of several irregular openings, it yields a fairly symmetric cavity. At this final stage of development shown in figure 1, the cavity's upper diameter is approximately forty times as wide as the defect aperture. Cavity volume is calculated based on fitting a conical cavity profile to the **lower** and **upper diameters**, denoted as *d* and *D*, respectively.
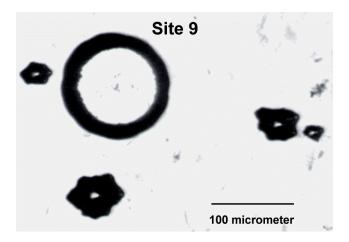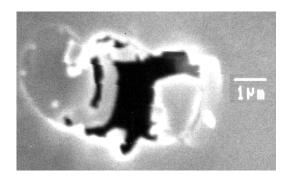

Fig. 1: Neighborhood of undercut cavity, site 9.

Fig. 2: Defect aperture at site 9.

3. NUMERICAL SIMULATION

In order to provide a comparison to the asher data, a quasi three-dimensional computational model was developed and coded to simulate AO undercutting at defect sites in protective coatings. The impact of AO collisions with the cavity wall is treated using an iterative process. For a given time step, the erosion yield for a unit of AO flux is calculated based on the current specified probabilities and cavity geometry. The yield is calculated by summing the contributions of successive reactive collisions until the flux is effectively extinguished either by recombination and reactive collisions at the cavity surface or by efflux at the defect. The cavity volume is updated based on the computed yield, and the iteration proceeds to the next time step by introducing a new unit of flux.

The modeling is simplified by assuming that isotropic AO flux incident on a circular defect etches a conical cavity, consistent with the experimental model for volume estimation. It is emphasized that volume erosion by undercutting is basically a surface activity that proceeds incrementally, similar to successively removing thin layers from an onion-half, starting at the inner ring. For the case of low energy plasma asher AO, the average "successful" AO atom undergoes hundreds or even thousands of collisions with the cavity interior before chemically reacting. To increase the computational efficiency of the model, the cavity surface is treated as having a homogeneous composition. This is a very good approximation because collisions randomize the AO distribution, and the frequency that different cavity surface elements are struck by AO is essentially in direct proportion to their relative surface areas. Thus, in each computational collision, the AO atoms are considered to collide collectively with an ideal surface having the surface-averaged properties representative of the actual glass coating area, polyimide Kapton® area, and defect area. Additional simplification is obtained by using effective average values to account for complex physical phenomena, as in the case of AO reaction with the polymer molecules. The AO reaction probability at Kapton®, P_r, probability of AO recombination at glass surfaces resulting in O_2, P_{cg}, and recombination at the polymer surface, P_{ck}, are prescribed and handled as stationary parameters. These parameters are specified along with the sample thickness, h_k, defect radius, r_{def}, and AO fluence, F.

4. DISCUSSION OF RESULTS

SEM measurements of defect size were obtained at 30 protective coating sites on the same sample as studied in [5]. The total ashing time for the sample was 1306 hr, which was carried out over a period of two months consisting of 21 separate ashing sessions. The effective AO fluence, as determined by the witness-coupon mass lost through etching over the ashing period of 1306 hr, is equivalent to a fluence of 1.96×10^{22} atom/cm^2.

Until the cavity expands to reach the lower coating, the only measurable variable is the upper diameter, D. It is assumed that the cavity depth, h, equals the upper cavity radius while it is growing, up to the instant it reaches the lower protective coating. This assumption is convenient and reasonably consistent with the data. The **thickness of the Kapton® film is denoted by h_k**. Because the defects are irregular in shape, the radius of a circle with the same area as the defect area is used as the effective radius of the defect. The effective radii in this report are presented in terms of h_k and range between approximately 0.005 and 0.2 h_k.

The volume, V, of revolution corresponding to the assumed linear-arc cavity profile is given by equation (1). The expression is for a truncated cone of height h with base diameters d and D, and reduces to a cone for $d = 0$.

$$V = \frac{\pi h}{12}\left(D^2 + Dd + d^2\right) \tag{1}$$

In the numerical simulation of erosion ($d = 0$, $D < 2\,h_k$), finite d is given in terms of D by the following equation

$$d = D - 2h_k\left(D/2h_k\right)^{-0.324}, \qquad D \geq 2h_k. \tag{2}$$

This relationship between the diameters was determined by fitting the experimental data for the sites studied. The variation in d with respect to D is given in figure 3 where **dimensions are given in units of the Kapton® sample thickness, h_k** = 0.0254 mm. The dotted curve in this figure represents the limiting condition $d = D$. Inspection of the data trend reveals that the difference between D and d decreases slowly for increasing D. As explained in the numerical simulation section, the amount of volume erosion is determined by the yield per unit of AO flux at a given time step and this is determined numerically in terms of the parameters listed in that section. Similarly, the increase in volume over a time step obviously results in an associated increase in $D,$ and perhaps d. The fractional composition of the cavity surface, composed of polymer area, glass area and defect area, is easily updated as functions of newly computed diameters.

The following material compares the principal experimental and numerical findings. SEM measurements were made of the defects at eight sites that had been monitored over the entire ashing sequence. For these cavity sites the volume erosion gain at three fluence levels is presented in figure 4 as a function of defect radius (given in units of Kapton® film thickness, h_k). Erosion gain, G, is computed by dividing the volume of erosion, V, produced by undercutting below a given defect area, A_{def}, by the volume, V_w, of erosion resulting from exposing an equivalent area of unprotected witness material to identical fluence. For witness area, A_w, not equal to A_{def}, gain is calculated as given by the equation

$$G \;=\; \frac{V}{V_W} \cdot \frac{A_W}{A_{def}} \tag{3}$$

The results shown in figure 4 reveal that this undercutting erosion proceeds at significantly greater rates than unprotected erosion. The gain accelerates with decreasing defect size, with gains of a few hundred achievable for $r_{def} < 0.02\ h_k$ at final fluence. It is emphasized that the gain increases for all sites upon increasing AO fluence, with a greater percentage arising from the earlier fluence stage.
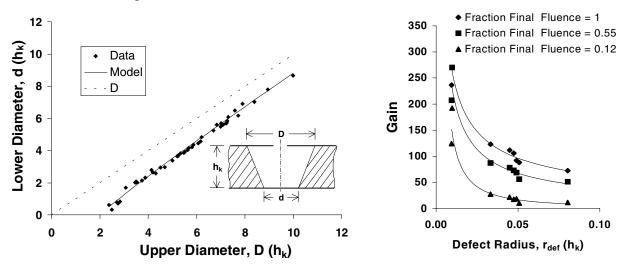

Fig. 3: Variation of d with D.   Fig. 4: Erosion gain versus defect radius.

To supplement the sites that had been studied at regular fluence intervals, SEM measurements were taken of additional sites after the final ashing session. The volumes of these sites were calculated only for final fluence. The dependence of erosion gain at the final fluence upon defect size is presented in figure 5 for all the resolvable defects. The combined results substantiate that the efficiency of undercutting accelerates with reduction of defect size.

One factor for the increase in erosion compared to unprotected Kapton$^{®}$ is geometric in nature. The undercut cavity serves as a trap for AO atoms that do not react initially. Given a low enough probability for recombination, the AO is afforded many more collisions to chemically react before exiting the cavity. Smaller defects provide cavities that are geometrically more efficient at trapping AO because effluence is lower. As the size of the defect area becomes large compared to h_k, the gain approaches unity. The exact variation of gain with defect size is complicated and depends on the rates of reaction and recombination. The experimental variation in gain is compared with numerical simulation results using the same h_k and similar r_{def}.

Because the actual values of the probabilities P_r, P_{ck}, and P_{cg} are unknown, they must be specified somewhat arbitrarily. To reduce the number of independent variables, results are presented only for $P_{ck} = P_{cg} \equiv P_c$. The numerical specification of probabilities starts by first selecting a desired value of G, say, to match an experimental G for a given fluence, F, and r_{def}. Next, with P_c set to zero, an estimated value for P_r is used, resulting in a cavity giving approximately the desired gain. By trial and error, P_r is adjusted until the desired value of G is obtained. The process is repeated for nonzero values of P_c, resulting in new values of P_r. Table I shows an array of values for P_r and P_c that maintains $G = 145$ for $F = 1.96 \times 10^{22}$ atom/cm^2 and $r_{def} = 0.03$ h_k. This value of G was chosen by fitting to the experimental data (near the knee of the curve) shown in figure 5. Also listed in this table are values of G for $r_{def} = 0.005$ h_k and $r_{def} = 0.2$ h_k, selected so as to span the experimental range of defect size. By examining the table, it can
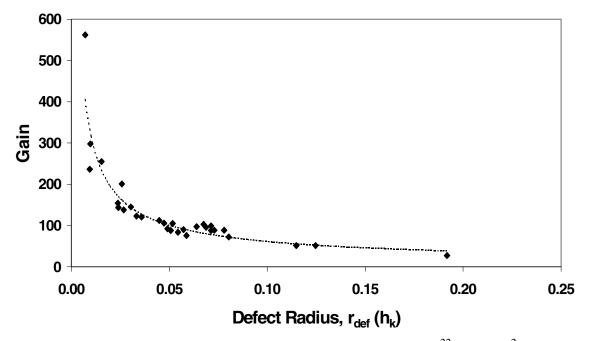

Fig. 5: Gain versus defect radius at final fluence, 1.96×10^{22} atom/cm^2.

be seen that decreasing P_r results in an increase in G for $r_{def} = 0.005\ h_k$ and a decrease in G for $r_{def} = 0.2\ h_k$. The reason for this dissimilar variation in gain with defect size can be explained in terms of relative influence of P_r and P_c upon G. For constant defect size, an increase in either P_r or P_c decreases G, and thus, to maintain a constant G, if one probability is increased then the other must be decreased. In terms of the tabulated results for the case $r_{def} = 0.005\ h_k$, the increased gain achieved at lower values of P_r evidently more than offsets the decrease in gain due to higher values of P_c. This is not true for the case $r_{def} = 0.2\ h_k$. This explains the tabulated "see-saw" variation of G with r_{def} about the maintained value of 145 at $r_{def} = 0.03\ h_k$. Little change in G occurs for $P_r < 0.0001$. The variation in G over the range of r_{def} is about a factor of three.

Table I: Simulated gain for three defect sizes for various P_r and $P_{ck} = P_{cg}$.				
Probability of Reaction, P_r	Probability of Recombination, P_c	$r_{def} = 0.005\ h_k$	$r_{def} = 0.03\ h_k$	$r_{def} = 0.2\ h_k$
		Gain		
0.006089	0	158.1	145	84.2
0.001	0.00287	163.1	145	53.3
0.0001	0.00337	164.4	145	50.7
0.00001	0.00342	164.5	145	50.5

To compare the results, gain values in Table I for $P_r = 0.001$ ($P_c = 0.00287$) are presented with the experimental values in figure 6. The scale of each axis is logarithmic. The experimental data vary approximately linearly on this scale, whereas the simulated results reveal a concave trend in the curve for smaller r_{def}.

To illustrate the dynamic variation of G with F, experimental values and simulated results are shown in figure 7 for three common values of r_{def}. G increases, in general, at a more gradual rate for the experimental data as compared to the simulated data. While suitable choices of P_r and P_c can be made to produce a simulated gain that is in exact agreement with the experimental data for a given fluence and defect size, considerable departure from the experimental data exists elsewhere. Variations of approximately a factor of two in gain are observed but not unexpected. It should be noted that the capability of specifying unequal combinations of P_{ck} and P_{cg} results in an additional parameter beyond that used here to explore simulated results. By varying the ratio of P_{cg} to P_{ck}, simulated results can be obtained that are more "in line" with the experimental. The explanation for this added capability to "tune" simulated results is that the fractional cavity area composed of glass surface increases with cavity size. For higher ratios of P_{cg} to P_{ck}, the larger the cavity the more its gain will be reduced below the level obtained when using equal recombination probabilities, $P_{cg} = P_{ck}$, because a larger cavity has a surface composition having a higher fractional glass area, resulting in higher AO loss through recombination.

Factors other than defect size influence cavity shape and evolution. These factors may act independently or in concert in a complex fashion. For example, the shape or size of a cavity may regulate reaction rates or chemical concentrations, leading to a non-uniform or nonlinear growth process. This may be the result of geometry, chemistry, transport phenomena or other physical phenomena. Nevertheless, the extent of agreement between the experimental and simulated results suggest that the increased erosion rates of undercutting erosion over open erosion can be explained to a great extent on the basis of geometric trapping.
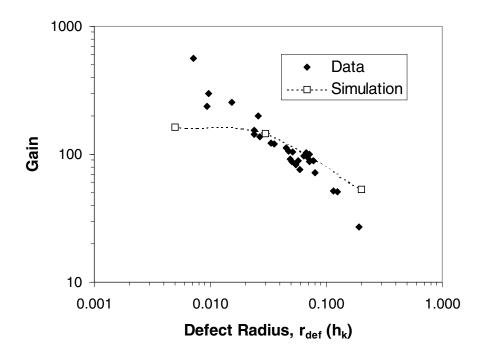
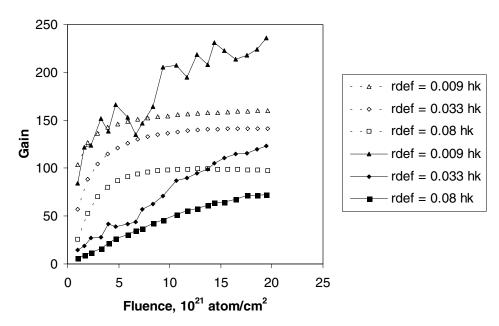Fig. 6: Comparison of experimental and simulated gain for various defect sizes.

Fig. 7: Experimental (solid) and simulated (open) gain versus
AO fluence for several defect sizes.

5. SUMMARY AND CONCLUSIONS

Undercutting erosion below pin widow defect sites in the SiO_x protective coating of polyimide Kapton® H thin film (0.0254 cm) was studied. The upper surface of the protective coating was subjected to the low energy isotropic AO flux produced in a plasma asher for a period equivalent to an effective in-space AO fluence of 1.96×10^{22} atoms/cm^2. Numerous cavity sites were examined during a sequence of twenty-one ashing sessions. Cavity diameters were measured and conical cavity volumes were calculated based on fitting linear profiles. SEM measurements were made to determine defect size. A quasi three-dimensional numerical code, which characterizes AO collisions with the wall in a collective manner, was also used to calculate undercutting erosion.

Volume erosion gain was calculated for undercut cavities based on erosion of unprotected material for both the experimental data and numerically simulated data. It was found that the gain increases significantly as a cavity develops; a larger fluence results in a larger cavity that better "traps" the AO atoms, producing a greater volume erosion yield per atom. For both sets of data, gain increases with decreasing defect size but is more pronounced in the experimental data. For the simulated data, the increase in gain for the smaller defects moderates with continued reduction in size. In general, for small AO fluence (small cavities) and large defects erosion gain is close to one, but for larger fluence and smaller defects, erosion gains of a few hundred are obtained. Based on this study, erosion gain is a dynamic quantity that depends primarily on defect size and AO fluence and is explained to a good degree in terms of the geometric trapping of AO.

REFERENCES

[1]   B.A. Banks, B.M. Auer, S.K. Rutledge, and C.M. Hill, "Atomic Interaction with Solar Array Blankets at Protective Coating Defect Sites," presented at the *4th Annual Workshop on Space Operations, Automation and Robotics (SOAR 90)*, NM, June 1990.

[2]   B.A. Banks, S.K. Rutledge, K.K. de Groh, B.M. Auer, and C.M. Hill "Atomic Oxygen Protective Coatings," presented at the *NATO Advanced Study Institute Conference*, Pitlochry, Scotland, July 1991.

[3]   B.A. Banks, K.K. de Groh, S.K. Rutledge, and F. DiFilippo, "Prediction of In-space of Durability Protected Polymers Based on Ground Laboratory Energy Atomic Oxygen," *NASA Technical Memorandum TM 107209*, 1996.

[4]   B.A. Banks, T.J. Stueber, S.A. Snyder, S.K. Rutledge, and M.J. Norris, "Atomic Oxygen Erosion Phenomena," presented at the *American Institute of Aeronautics and Astronautics Defense and Space Programs Conference*, Alabama, September 1997.

[5]   A. Snyder, "Investigation of Atomic Oxygen Erosion of Polyimide Kapton® H Exposed to a Plasma Asher Environment," presented at the 44th International SAMPE Symposium and Exhibit, Long Beach, California, May 23–27, 1999.

[6]   A.S. da Silva Sobrinho, G. Czeremuszkin, M. Latreche, M.R. Wertheimer, "A Study of Defects in Ultra-thin Transparent Coatings on Polymers," Applied Physics A 67, 1–3 (1998).

[7]   A.S. da Silva Sobrinho, M. Latreche, G. Czeremuszkin, J.E. Klemberg-Sapieha, M.R. Wertheimer, "Transparent Barrier Coatings on polyethylene Terephthalate by Single and Dual-Frequency Plasma-Enhanced Chemical Vapor Deposition," J. Vacuum Science Technology A 16(6), Nov./Dec. (1998).

REPORT DOCUMENTATION PAGE

1. AGENCY USE ONLY (Leave blank)	2. REPORT DATE	3. REPORT TYPE AND DATES COVERED
	June 2001	Technical Memorandum

4. TITLE AND SUBTITLE

The Dependence of Atomic Oxygen Undercutting of Protected Polyimide Kapton® H Upon Defect Size

5. FUNDING NUMBERS

WU–755–A4–13–00

6. AUTHOR(S)

Aaron Snyder and Kim K. de Groh

7. PERFORMING ORGANIZATION NAME(S) AND ADDRESS(ES)

National Aeronautics and Space Administration
John H. Glenn Research Center at Lewis Field
Cleveland, Ohio 44135–3191

8. PERFORMING ORGANIZATION REPORT NUMBER

E–12554

9. SPONSORING/MONITORING AGENCY NAME(S) AND ADDRESS(ES)

National Aeronautics and Space Administration
Washington, DC 20546–0001

10. SPONSORING/MONITORING AGENCY REPORT NUMBER

NASA TM—2001-210596

11. SUPPLEMENTARY NOTES

Prepared for the Eighth International Symposium on Materials in a Space Environment and the Fifth International Conference on Protection of Materials and Structures for LEO Space Environment cosponsored by the CNES, ITL, Inc., ESA, ONERA, and the CSA, Arcachon, France, June 5–9, 2000. Responsible person, Aaron Snyder, organization code 5480, 216–433–5918.

12a. DISTRIBUTION/AVAILABILITY STATEMENT

Unclassified - Unlimited
Subject Categories: 18 and 27   Distribution: Nonstandard

Available electronically at http://gltrs.grc.nasa.gov/GLTRS

This publication is available from the NASA Center for AeroSpace Information, 301–621–0390.

12b. DISTRIBUTION CODE

13. ABSTRACT (Maximum 200 words)

Understanding the behavior of polymeric materials when exposed to the low-Earth-orbit (LEO) environment is important in predicting performance characteristics such as in-space durability. Atomic oxygen (AO) present in LEO is known to be the principal agent in causing undercutting erosion of SiO_x protected polyimide Kapton® H film, which serves as a mechanically stable blanket material in solar arrays. The rate of undercutting is dependent on the rate of arrival, directionality and energy of the AO with respect to the film surface. The erosion rate also depends on the distribution of the size of defects existing in the protective coating. This paper presents results of experimental ground testing using low energy, isotropic AO flux together with numerical modeling to determine the dependence of undercutting erosion upon defect size.

14. SUBJECT TERMS

Oxygen atoms; Protective coatings; Erosion

15. NUMBER OF PAGES

15

16. PRICE CODE

17. SECURITY CLASSIFICATION OF REPORT	18. SECURITY CLASSIFICATION OF THIS PAGE	19. SECURITY CLASSIFICATION OF ABSTRACT	20. LIMITATION OF ABSTRACT
Unclassified	Unclassified	Unclassified	